A STUDY ON ATMOSPHERIC BOUNDARY-LAYER CHARACTERISTICS AT ANAND, INDIA USING LSP EXPERIMENTAL DATA SETS

A. N. V. SATYANARAYANA[1], V. N. LYKOSSOV[2] and U. C. MOHANTY[1,⋆]
[1]*Centre for Atmospheric Sciences, Indian Institute of Technology, New Delhi, India;* [2]*Institute of Numerical Mathematics, Moscow, Russia*

(Received in final form 6 October 1999)

Abstract. An attempt is made to study the planetary boundary layer (PBL) characteristics during the winter period at Anand (22.4°N, 72.6°E), a semi-arid region, which is located in the western part of India. A one-dimensional turbulent kinetic energy (TKE) closure model is used for the study. The structure of the PBL, which consists of profiles of zonal and meridional components of wind, potential temperature and specific humidity, is simulated. A one-dimensional soil heat and moisture transport parameterization scheme is incorporated for the accurate representation of the energy exchange processes at the soil-atmosphere interface. The diurnal variation of fluxes of sensible heat, latent heat, shortwave radiation, net radiation and soil flux, soil temperature at different depths, Richardson number and TKE at the height of the constant flux layer is studied. The model predictions are compared with the available observations obtained from a special Land Surface Processes (LSP) experiment.

Keywords: Fluxes, Land surface processes, Planetary boundary layer, Turbulent kinetic energy.

1. Introduction

The important role of land surface processes in weather and climate has been recognized during the last few years. The coupling of land surface processes with the atmosphere occurs through the exchange of heat, momentum and moisture. Biospheric processes also play a vital role in influencing these exchanges (Mihailovic et al., 1981; Sellers et al., 1986; Noilhan and Planton, 1989; Volodin and Lykossov, 1998). Raman et al. (1998) have investigated the influence of soil moisture and vegetation variations on simulations of monsoon circulation and rainfall by incorporating a simple land surface parameterization scheme (Noilhan and Planton, 1989) in a three-dimensional, high resolution, regional, nested-grid, atmospheric model. The exchange processes in the atmospheric surface layer and soil result from complex interaction between them. This requires a proper parameterization of heat and moisture transfer at the land surface and in the soil, and should be incorporated within the planetary boundary layer (PBL) models to improve the efficiency of characterizing the boundary-layer processes.

⋆ *Author for correspondence*: Prof. U.C. Mohanty, Centre for Atmospheric Sciences, Indian Institute of Technology, Hauz Khas, New Delhi - 110 016, India, E-mail: mohanty@cas.iitd.ernet.in

Boundary-Layer Meteorology **96:** 393–419, 2000.

Several studies on the PBL in India have been reported using the observational data of MONTBLEX (Monsoon Trough Boundary-Layer Experiment), which was conducted along the monsoon trough region, during the southwest summer monsoon season of 1990. The focus of this experiment is to study boundary-layer processes during different stages of the summer monsoon and to study the role played by moist and dry convection in the evolution of the boundary layer with a view to parameterizing the surface fluxes of heat, moisture and momentum for application in weather prediction models. Vernekar et al. (1991, 1993) have studied the structure and growth of the boundary layer and its characteristics. Tyagi et al. (1994) have attempted to study the structure of the PBL in the monsoon trough region. Parashuram et al. (1994) simulated the thermodynamic structure of the atmospheric boundary layer using a one-dimensional turbulent kinetic energy (TKE) closure PBL model. Kusuma et al. (1995) have studied the turbulent heat flux variation over the monsoon trough regime. Kusuma et al. (1996) used an one-dimensional model with TKE-turbulence scale and TKE-ϵ closures to simulate the monsoon trough boundary layer. They found that the choice of the constants in the dissipation equation is a crucial issue, and suggested a set of values that avoids a common approximation for TKE generation and actually simulates the turbulence structure better. The evolution and structure of the associated boundary-layer processes were examined by Potty et al. (1996) using a high resolution primitive equation model.

Very few studies are conducted on land surface processes in India, leading to a paucity of data. To fill this gap, a multi-institutional Land Surface Processes (LSP) experiment was conducted at Anand (22.4°N, 72.6°E) in 1997. In the present paper an attempt is made to simulate the boundary-layer characteristics by using a one-dimensional PBL model with the TKE-ϵ closure scheme and a soil heat and moisture transport model. The simulated boundary-layer characteristics consist of fluxes of sensible heat, latent heat, shortwave radiation and net radiation; turbulent kinetic energy; ABL height; Obukhov length scale; Richardson number; profiles of zonal and meridional components of wind, potential temperature and specific humidity. Soil characteristics such as temperature at different depths and heat flux at 5 cm depth are also simulated. These simulated values are compared with the available observations from the LSP experiment.

2. Data

The multi-institutional Land Surface Processes (LSP) experiment was conducted at Sabarmati Basin Area, Gujarat, in the Western part of India, in 1997. Five experimental platforms were chosen, namely Anand (central station), Sanad, Arnej, Khandha and Derol, covering an area of 100×100 km^2. All these stations were equipped with 9-m towers. Meteorological sensors for wind direction, wind speed, temperature and humidity were erected at 1, 2, 4 and 8 m heights on the towers.

Sensors for measuring pressure, precipitation, evaporation, soil temperature at different depths, radiation (shortwave, longwave and net radiation) and soil heat flux were also used. These instruments were connected to a data module for storing. To derive the vertical wind profile, pilot balloon ascents were taken at 0000 and 1200 UTC at these stations.

At Anand special radiosonde (RS/RW) ascents were conducted by the India Meteorological Department (IMD), during the Intensive Observational Periods (IOP). The frequency of observations was 0000 UTC, 0300 UTC, 0600 UTC, 0900 UTC and 1200 UTC. The IOP was for a period of 6 days in every month.

In this study, IOP data during 14–17 February, 1997 at Anand are utilized. The data consist of observations of temperature and zonal and meridional components of wind at 1, 2, 4 and 8 m height and relative humidity at 2 and 4 m height from a 8-m tower, and surface pressure. Upper air observations of temperature, dew point temperature, wind speed and direction at different pressure levels up to 700 hPa are considered as input in the PBL model. No precipitation was observed during this time period. The data also include soil type and texture, soil temperature at the surface, 5 cm, 10 cm, 20 cm, 40 cm and 100 cm depth, incoming solar radiation, longwave radiation, reflected incoming solar radiation, soil heat flux at 5 cm depth and surface soil moisture.

The meteorological tower at Anand was located in the midst of an agricultural farm. This region is a flat river basin area and is situated in the semi-arid/arid zone of the western part of India in nearly homogeneous terrain. Low-level crops were present during the experimental period. No significant weather activity was noticed and no precipitation occurred during the study period. Advection components are found to be small over this area, verified by NCMRWF (National Centre for Medium Range Weather Forecasting) large-scale analyses. Thus the conditions are well suited for applying a 1-D model to understand the land-surface processes and boundary-layer characteristics at Anand.

3. Model Formulation

All calculations presented in this work are performed with a one-dimensional TKE-ϵ closure model, which includes effects of the horizontal advective transport of heat and moisture. Additionally, prognostic equations for the soil heat and moisture diffusion are used. Since the simulation is made for a semi-arid region during the winter period, a rather simple approach for computing soil moisture is applied, though it is known (Pielke, 1984; Volodin and Lykossov, 1998) that, generally, the transfer processes in soil are highly non-linear. The model has 40 levels in the vertical, with $\Delta Z = 50$ m from 8 m to 1958 m. The soil layer from the surface to 2 m depth is considered with 40 levels in the downward direction.

TABLE I
Overview of the model.

Model Description	1-D PBL (TKE-ϵ) + Soil heat and moisture transporation model
Vertical domain	-2 to 2000 m
Vertical levels	40, Δz = 50 m
Levels under the surface	40, Δz = 0.05 m
Independent variables	z, t
Prognostic variables	$u, v, \theta, q, q_w, E, \epsilon, T_{\text{soil}}, q_{\text{soil}}$
Diagnostic variables	K_u
Numerical scheme	Second order accuracy
Time integration	Implicit, Δt = 600 sec
Boundary conditions	For lower boundary, Monin–Obukhov similarity theory is applied
	For upper boundary, the geostrophic conditions, actual observed meterological values at 2000 m; for TKE, ϵ, zero flux at 2000m are considered
	For under the surface, soil heat and moisture diffusion processes are considered
Physical processes	Heat and moisture advection
	Water phase transitions
	Dry and moist convective adjustment
	Sensible and latent heat fluxes
	Longwave and shortwave radiation fluxes

3.1. MODEL EQUATIONS

In a Cartesian co-ordinate system, where the horizontal axes x and y are directed to the east and north respectively, and the vertical axis z is directed upward, the planetary boundary-layer equations can be written in the following form (Lykossov and Platov, 1992; Kusuma et al., 1996):

$$\frac{\partial u}{\partial t} = -\frac{\partial \overline{u'w'}}{\partial z} + fv - \tilde{p}_x/\tilde{\rho}, \tag{1}$$

$$\frac{\partial v}{\partial t} = -\frac{\partial \overline{v'w'}}{\partial z} - fu - \tilde{p}_y/\tilde{\rho}, \tag{2}$$

$$\frac{\partial \theta}{\partial t} + u\tilde{\theta}_x + v\tilde{\theta}_y = -\frac{\partial \overline{\theta'w'}}{\partial z} + Q_r + Q_f, \tag{3}$$

$$\frac{\partial q}{\partial t} + u\tilde{q}_x + v\tilde{q}_y = -\frac{\partial \overline{q'w'}}{\partial z} + E - C, \tag{4}$$

$$\frac{\partial q_w}{\partial t} + u\tilde{q}_{wx} + v\tilde{q}_{wy} = -\frac{\partial \overline{q'_w w'}}{\partial z} - E + C - P, \tag{5}$$

$$\frac{\partial p}{\partial z} = -g\rho, \tag{6}$$

$$p = \rho RT, \tag{7}$$

$$\theta = T(\frac{p_0}{p})^{R/c_p}. \tag{8}$$

Here, u, v and w are x-, y- and z-components of the wind velocity, θ is the potential temperature, T is the absolute temperature, q is the specific humidity, q_w is the specific liquid-water content, p is the pressure, ρ is the density of the air-water-water vapour mixture, $(\tilde{p}_x, \tilde{p}_y)$, $(\tilde{\theta}_x, \tilde{\theta}_y)$, $(\tilde{q}_x, \tilde{q}_y)$, and $(\tilde{q}_{wx}, \tilde{q}_{wy})$ are components of horizontal gradients of the pressure, potential temperature, specific humidity and specific liquid-water content in the free atmosphere, Q_r and Q_f are rates of the heating due to radiation and phase transitions of the water, C and E are rates of phase changes: water vapour $\rightarrow$ liquid water (condensation) and water $\rightarrow$ water vapour (evaporation), P is the precipitation rate, $\rho\overline{u'w'}$, $\rho\overline{v'w'}$, $c_p\rho\overline{\theta'w'}$, $\rho\overline{q'w'}$ and $\rho\overline{q'_w w'}$ are the vertical turbulent fluxes of momentum (u and v components), heat, water vapor and liquid water, R is the gas constant, c_p is the specific heat at constant pressure, $p_0 = 1000$ hPa is standard value of pressure, $f = 2\Omega \sin\phi$ is the Coriolis parameter (Ω is the angular earth's rotation velocity, ϕ is latitude), g is the acceleration due to gravity.

3.2. Parameterization of pressure forcing and advection

To compute the pressure gradient in Equations (1) and (2), the geostrophic wind relationships are used:

$$\tilde{p}_x/\tilde{\rho} = fv_g, \qquad \tilde{p}_y/\tilde{\rho} = -fu_g, \tag{9}$$

where u_g and v_g are assumed to be taken from observed profiles of the wind in the free atmosphere

$$u_g = u_{obs}(H,t) + \frac{\partial u_{obs}}{\partial z}|_{z=H}(z-H),$$

$$v_g = v_{obs}(H,t) + \frac{\partial v_{obs}}{\partial z}|_{z=H}(z-H). \tag{10}$$

Here, $z = H$ is the top of model domain, subscript *obs* refers to observed data. To compute the horizontal gradients of temperature, the thermal wind relationships are employed

$$\tilde{\theta}_x = \frac{f\theta_{obs}}{g}\left[\frac{\partial v_g}{\partial z} + \frac{g(1 + R/c_p)}{RT_{obs}}v_g\right],$$

$$\tilde{\theta}_y = -\frac{f\theta_{obs}}{g}\left[\frac{\partial u_g}{\partial z} + \frac{g(1 + R/c_p)}{RT_{obs}}u_g\right]. \tag{11}$$

It is also assumed that $\tilde{q}_{wx} = \tilde{q}_{wy} = 0$, and

$$\tilde{q}_x = \frac{\partial}{\partial x}\left[\tilde{r}q_{max}(\tilde{T}, \tilde{p})\right] \approx \tilde{r}\frac{\partial q_{max}(\tilde{T}, \tilde{p})}{\partial x} \approx \tilde{r}\frac{\partial q_{max}}{\partial \tilde{T}}\frac{\partial \tilde{T}}{\partial x} \approx$$

$$\tilde{r}\frac{\partial q_{max}}{\partial \tilde{T}}(\tilde{\theta}_x + \frac{f}{c_p}v_g), \tag{12}$$

where $r = q/q_{max}$ is the relative humidity. Similarly,

$$\tilde{q}_y \approx \tilde{r}\frac{\partial q_{max}}{\partial \tilde{T}}(\tilde{\theta}_y - \frac{f}{c_p}u_g). \tag{13}$$

3.3. TURBULENCE CLOSURE

In the model, the atmospheric boundary layer is partitioned into two subdomains: the near-surface constant-flux layer ($z \leqslant h$) and the free-atmosphere-topped "interfacial" layer ($h < z \leqslant H$). It is assumed that h and H do not vary in time. In order to calculate vertical turbulent fluxes of momentum, heat and moisture in the interfacial layer, the Boussinesq hypothesis is used

$$\overline{a'w'} = -K_a\frac{\partial a}{\partial z}, \tag{14}$$

where a is any of the prognostic variables u, v, θ, q and q_w, and K_a is the eddy exchange coefficient. It is assumed that $K_a = \alpha_a K$ where α_a is a dimensionless constant (equal to unity for the momentum flux). The coefficient K is related to the turbulent kinetic energy E and the dissipation rate ϵ by the Kolmogorov (1942) equation

$$K = \frac{C_k E^2}{\epsilon}, \tag{15}$$

where C_k is a dimensionless constant.

To compute E and ϵ, additional prognostic equations are used (Kusuma et al., 1996)

$$\frac{\partial E}{\partial t} = P - \epsilon - \frac{\partial \overline{w'E'}}{\partial z}, \tag{16}$$

$$\frac{\partial \epsilon}{\partial t} = P_\epsilon - D_\epsilon - \frac{\partial \overline{w'\epsilon'}}{\partial z}, \tag{17}$$

where

$$P = -\left(\overline{u'w'}\frac{\partial u}{\partial z} + \overline{v'w'}\frac{\partial v}{\partial z} + \frac{g}{\rho}\overline{\rho'w'}\right) \tag{18}$$

and $P_\epsilon = C_1 \epsilon P/E$ and $D_\epsilon = C_1 \epsilon^2/E$. Here, the dimensionless parameter C_1 is taken as suggested by Aupoix et al. (1989)

$$C_1 = \frac{\mathcal{C}}{1 + 0.69(2 - \mathcal{C})/\sqrt{Re}}, \qquad Re = \frac{(2E/3)^2}{\nu\epsilon}, \tag{19}$$

where ν is the air molecular viscosity, $\mathcal{C}$ is the universal constant (in the model, we used $\mathcal{C}$ = 1.9). Note that we used only one dimensionless parameter C_1 for this $E - \epsilon$ model unlike the standard one, in which two different coefficients of proportionaly are employed to parameterize P_ϵ and D_ϵ. Xu and Taylor (1997) pointed out that there is a tendency of the standard $E - \epsilon$ model to predict very large values of the dissipation length $l \sim E^{3/2}/\epsilon$ and the eddy viscosity K at large heights in neutral stratification. In our model, the proportionality coefficient C_1 is a function of E and ϵ. As found by Kusuma et al. (1996), this can automatically take care of the dissipation during both decaying and developing turbulence and provide reasonable magnitudes of l and K.

As above, to compute the turbulent fluxes of TKE and dissipation rate, the down-gradient hypothesis is used

$$\overline{w'E'} = -\alpha_E K \frac{\partial E}{\partial z}, \tag{20}$$

$$\overline{w'\epsilon'} = -\alpha_\epsilon K \frac{\partial \epsilon}{\partial z}, \tag{21}$$

where α_E and α_ϵ are dimensionless constants. We assumed that $\alpha_E = \alpha_\epsilon = 0.73$, and $\alpha_\theta = \alpha_q = \alpha_{q_w}$, the value of α_θ being calculated using the constant-flux layer theory.

Finally, the buoyancy flux term used in Equations (16) and (17) is calculated as

$$\frac{g}{\rho}\overline{\rho'w'} = -\frac{g}{\theta}\overline{\theta_v' w'}, \tag{22}$$

where $\theta_v = (1 + 0.61q - q_w)\theta$ is the virtual potential temperature. To calculate $\overline{\theta_v' w'}$, the following rather accurate approximation is used

$$\overline{\theta_v' w'} = \overline{\theta' w'} + \theta(0.61\overline{q' w'} - \overline{q_w' w'}). \tag{23}$$

3.4. RADIATION

An important process in the evolution of atmospheric boundary layer and in its interaction with the surface is radiation, which is described by the term Q_r in Equation (3). Without dwelling on the radiation scheme in the model, we point out that

$$\rho c_p Q_r = -\frac{\partial(F^{\downarrow} - F^{\uparrow})}{\partial z}, \tag{24}$$

where $F^{\uparrow}$ and $F^{\downarrow}$ stand for the total upwelling and downwelling radiative fluxes respectively. The model has both shortwave heating and longwave cooling effects. To calculate the radiative fluxes, the radiation scheme developed by Harshvardhan et al. (1987) has been used. Effects of water vapour, ozone and carbon dioxide are included in this parameterization. Additionally, the shortwave radiative flux is influenced by the underlying surface albedo and cloud albedo.

3.5. LOWER BOUNDARY CONDITIONS

The lower boundary of the interfacial layer is kept as the maximum height of the constant-flux layer. Then, the lower boundary conditions for the prognostic variables at the constant-flux layer height, $z = h$, are as follows

$$K\frac{\partial u}{\partial z} = C_D|\vec{V}_h|u_h, \tag{25}$$

$$K\frac{\partial v}{\partial z} = C_D|\vec{V}_h|v_h, \tag{26}$$

$$\frac{H_s}{c_p\rho} = -K_\theta\frac{\partial\theta}{\partial z} = -C_\theta|\vec{V}_h|(\theta_h - \theta_s), \tag{27}$$

$$\frac{E_s}{\rho} = -K_\theta\frac{\partial q}{\partial z} = -C_\theta|\vec{V}_h|(q_h - q_s), \tag{28}$$

where H_s and $\mathcal{L}E_s$ are the sensible and latent heat fluxes at the land surface, the subscript h indicates that the corresponding quantities refer to the upper boundary of the constant flux layer, the subscript s refers to the quantities determined at the air-soil interface. In Equations (25)–(28) we also used the notation $\vec{V} = (u, v)$.

The drag (C_D) and heat exchange (C_θ) coefficients are calculated on the basis of the Monin–Obukhov similarity theory

$$C_D = \frac{\kappa^2}{\left[\ln\left(h/z_0\right) - \psi_M\left(h/L\right)\right]^2}, \tag{29}$$

$$C_\theta = \frac{\alpha_\theta \kappa^2}{\left[\ln\left(h/z_0\right) - \psi_M(h/L)\right]\left[\ln\left(h/z_{0\theta}\right) - \psi_H(h/L)\right]}, \tag{30}$$

where z_0 and $z_{0\theta}$ are the momentum and heat roughness parameters, respectively, κ is the von Karman constant, and the Obukhov length L is defined as

$$L = -\frac{\theta u_*^3}{\kappa g \overline{\theta_v' w'}}, \tag{31}$$

where u_* is the friction velocity. The magnitude of $z_{0\theta}$ is controlled by transport mechanisms very close to the surface where molecular processes dominate. This is especially important under low-wind, unstable conditions. To calculate $z_{0\theta}$, the following approximation of experimental data obtained for natural and artificial surfaces is used (Garratt and Hicks, 1973; Kazakov and Lykossov, 1982):

$$\ln(z_0/z_{0\theta}) = \begin{cases} -2.43 & \text{for } Re_* \leqslant 0.111, \\ 0.83\ln(Re_*) - 0.6 & \text{for } 0.111 \leqslant Re_* \leqslant 16.3, \\ 0.49 Re_*^{0.45} & \text{for } Re_* \geqslant 16.3, \end{cases} \tag{32}$$

where $Re_* = u_* z_0/\nu$ is the roughness Reynolds number.

The integrated universal functions for momentum (ψ_M) and heat (ψ_H) are defined by

$$\psi_{M,H}(\zeta) = \int_0^\zeta \frac{1 - \phi_{M,H}(\zeta')}{\zeta'} d\zeta', \tag{33}$$

where $\zeta = z/L$ and $\zeta \gg \max(z_0, z_{0\theta})/L$ is assumed (Pielke, 1984). The stability functions $\phi_M(\zeta)$ and $\phi_H(\zeta)$ for the case of stable stratification are linear functions

$$\phi_M = \phi_H = 1 + \beta\zeta,$$

where the parameter β varies, according to observations, from 4.7 to 5.2. In this case

$$\psi_{M,H} = -\beta\zeta. \tag{34}$$

For regions with moderate unstable stratification ($-2 \leqslant \zeta \leqslant 0$), the Businger–Dyer formulations are used (Businger et al., 1971)

$$\phi_M = (1 - \alpha\zeta)^{-1/4}, \quad \phi_H = (1 - \alpha\zeta)^{-1/2}, \tag{35}$$

where suggested values of α range from 16 to 28. The corresponding integrated universal functions have the following form (Paulson, 1970)

$$\psi_M(\zeta) = \ln\left[\frac{1}{8}\left(1+\phi_M^{-2}\right)\left(1+\phi_M^{-1}\right)^2\right] - 2\arctan\phi_M^{-1} + \pi/2,$$
$$\psi_H(\zeta) = 2\ln\left[\frac{1}{2}\left(1+\phi_H^{-1}\right)\right]. \tag{36}$$

When convection dominates so that ζ is large and negative (in particular, in the case of light winds), the universal functions should vary as $(-\zeta)^{-1/3}$, a relation called the free-convection condition. Carl et al. (1973) suggested for momentum that

$$\phi_M = (1-16\zeta)^{-1/3}, \tag{37}$$

which satisfies to this condition when $-\zeta$ becomes large. The corresponding integrated universal function can be written as follows

$$\psi_M = \frac{3}{2}\ln\left[\frac{1}{3}(X^2+X+1)\right] - \sqrt{3}\left(\arctan\frac{2X+1}{\sqrt{3}} - \frac{\pi}{3}\right), \tag{38}$$

where $X = (1-16\zeta)^{1/3}$. A similar $-1/3$ power law dependence is also required for ϕ_H in order to satisfy the theoretical prediction. We combine the Businger-Dyer expressions and free-convection limit (Kazakov and Lykossov, 1982; Large et al., 1994; Fairall et al., 1996) to give

$$\phi_a = (b_a - c_a\zeta)^{-1/3} \quad \text{for } \zeta < \zeta_a, \tag{39}$$

where a stands for M or H, and the b_a and c_a are chosen so that both ϕ_a and its first derivative are continuous across the matching value $\zeta = \zeta_a$.

Finally, we formulate lower boundary conditions for the dissipation rate (Panofsky and Dutton, 1984)

$$\epsilon = \frac{u_*^3}{\kappa h}[\phi_M(h/L) - h/L], \tag{40}$$

and for TKE (Stull, 1988)

$$E = \begin{cases} 3.75u_*^2 & \text{for } h/L \geqslant 0, \\ [3.75 + (-h/L)^{\frac{2}{3}}]u_*^2 + 0.4w_*^2 & \text{for } h/L < 0, \end{cases} \tag{41}$$

where w_* is the Deardorff convective velocity scale

$$w_* = \left(\frac{g}{\theta}h_{pbl}\overline{w'\theta'_{vs}}\right)^{1/3}. \tag{42}$$

Here, h_{pbl} is depth of the convective boundary layer.

3.6. SOIL HEAT AND MOISTURE TRANSPORT MODEL

To compute the surface temperature, θ_s, and specific humidity, q_s, the surface energy and water budget equations are used

$$H_s + \mathcal{L}E_s + B_s = R_n,$$
$$E_s + W_s = P, \tag{43}$$

where R_n is the surface net radiation, $\mathcal{L}$ is the latent heat of vaporization, B_s is the soil surface heat flux, and W_s is the soil surface water flux. Additionally, the surface specific humidity is specified as follows:

$$q_s = r_s q_{max}(T_s, p_s), \tag{44}$$

where r_s is the surface relative humidity, q_{max} is the saturated value of specific humidity. To calculate B_s and W_s we employ the following prognostic equations for soil heat and moisture diffusion (the axis z is directed downward)

$$\rho_s c_{ps} \frac{\partial T_{soil}}{\partial t} = \frac{\partial}{\partial z} \lambda_T \frac{\partial T_{soil}}{\partial z},$$
$$\frac{\partial q_{soil}}{\partial t} = \frac{\partial}{\partial z} D_v \frac{\partial q_{soil}}{\partial z}, \tag{45}$$

where T_{soil} is the soil temperature, q_{soil} is the soil humidity, ρ_s is the soil density, c_{ps} is the soil specific heat, λ_T is the soil heat conductivity coefficient, D_v is the soil moisture diffusivity coefficient. Then, the fluxes B_s and W_s are defined as follows

$$B_s = -\lambda_T \frac{\partial T_{soil}}{\partial z}|_{z=0}, \qquad W_s = -D_v \frac{\partial q_{soil}}{\partial z}|_{z=0}.$$

The surface relative humidity r_s is calculated accordingly to DKRZ (1992) as

$$r_s = \frac{1}{2} \max \left[1 - \cos \left(\frac{\pi q_{soil}|_0}{\Pi} \right), 2 \min(1, r_h) \right],$$

where Π is the soil porosity, r_h is the relative humidity at the constant-flux layer height.

The prescribed values of temperature and specific humidity at the soil bottom are used as the soil lower boundary condition.

3.7. UPPER BOUNDARY CONDITIONS

The maximum height of the turbulent boundary layer (top of the PBL) is chosen as the upper boundary. At the top of the boundary layer, the wind speeds, the potential temperature and the moisture attain the observed values at that height. The TKE flux and dissipation flux are assumed to vanish at that height. Accordingly, at $z = H$,

$$u = u_{obs}(H, t), \quad v = v_{obs}(H, t), \quad \theta = \theta_{obs}(H, t), \quad q = q_{obs}(H, t),$$

$$\frac{\partial E}{\partial z} = 0, \quad \frac{\partial \epsilon}{\partial z} = 0.$$

The time variations of quantities with the subscript *obs* are obtained by the linear interpolation of the upper air measurements.

4. Numerical Experiment

The initial values

$$u = u_{obs}(z, 0), \quad v = v_{obs}(z, 0), \quad \theta = \theta_{obs}(z, 0), \quad q = q_{obs}(z, 0), \tag{46}$$

are prepared using the 0300 UTC slow rising RS/RW balloon data of 14th February, 1997 at Anand. The initial values at model grid points are obtained by linearly interpolating the high resolution vertical profile data which consist of zonal and meridional wind components, temperature and specific humidity. The interpolated values of these parameters at every 50 m in the vertical from 8 m (assumed height of the constant flux layer h) to 1958 m (top of the model domain) are given as input to the model. At $z = h$ the observations from the micro-meteorological tower are prescribed.

The lower boundary conditions are prepared using the three-hourly surface and micrometeorological tower observations at Anand, which consist of surface temperature, surface pressure and surface relative humidity. The time variation of these boundary conditions at every time step was obtained by linear interpolation in time. The observations at the top of the model domain were also interpolated in time and prescribed as upper boundary conditions.

For the radiation parameterization scheme incorporated in the model, climatological ozone data are prescribed.

The sub-surface boundary condition for the Soil Heat and Moisture Transport model, such as soil bottom temperature and specific humidity, are obtained from observations.

The model is integrated for 75 hours with a time step of 600 seconds (a total of 450 time steps). The model simulation of vertical profiles of zonal and meridional wind components, potential temperature, specific humidity for every hour are stored for the comparison purposes.

5. Results and Discussion

The results consist of the simulations of vertical profiles of zonal and meridional components of wind, potential temperature and specific humidity at Anand. The model also generated sensible heat, latent heat, shortwave radiation, net radiation and soil fluxes, boundary-layer height, turbulent kinetic energy, dissipation and Ri. The model gives hourly simulations, and the simulations were compared with the available observations. The observed profiles of zonal and meridional wind components, potential temperature and specific humidity obtained from RS/RW observations are linearly interpolated in the vertical and values at every 50 m interval up to 2000 m were used to compare with the simulations. The model simulations of vertical profiles of zonal and meridional wind components, potential temperature and specific humidity at different simulation hours are so chosen to verify the performance of the model at different times of a day.

Numerical experiments are conducted using different PBL parameterizations such as the Beljaars and Holtslag (1991) method, Businger–Dyer profiles for unstable stratification with and without advection and considering $z_{0\theta} = z_0$. The model predictions of vertical profiles of zonal and meridional wind components, potential temperature, specific humidity and turbulence characteristics of these numerical experiments are intercompared. Simulated vertical profiles of zonal and meridional wind components, potential temperature and specific humidity at 1200 UTC on 16th February 1997 are presented in Figures 1a–d and compared with the observations. It is seen that all these simulations are found to be more or less similar in nature with respect to each method and with the observations. The rest of the results presented are the simulations using the universal functions with advection as explained earlier in Section 3.

The vertical profiles of model simulations and observations of zonal wind on 14th February at 0900 UTC; 15th February at 0000 UTC; 16th February at 1200 UTC; 17th February at 0300 UTC (corresponding simulation hours and local time were presented in Table 2) are depicted in Figures 2a– 2d. It is noticed from Figures 2a, 2c and 2d that the model simulations are in good agreement with the observations. Model simulations reveal a maximum deviation of 6 m s^{-1} in Figure 2b with respect to observations, but the orientation of the simulated profile matched the observations.

Similarly, meridional wind profiles at the above mentioned hours are presented in Figures 3a–3d. Model predictions in Figure 3a are well-matched with the observations. Some deviations are observed in Figures 3b, 3c and 3d. The orientation of the simulated profiles in Figure 3b and Figure 3d matches the observations. The simulated profile reveals a maximum deviation of 5 m s^{-1} in Figure 3d at 500 m height while from 1150 m upwards the simulations are matching well with the observations.

The potential temperature profiles are presented in Figures 4a–4d. The model captured the superadiabatic lapse rate conditions well in Figure 4a. A steep near-

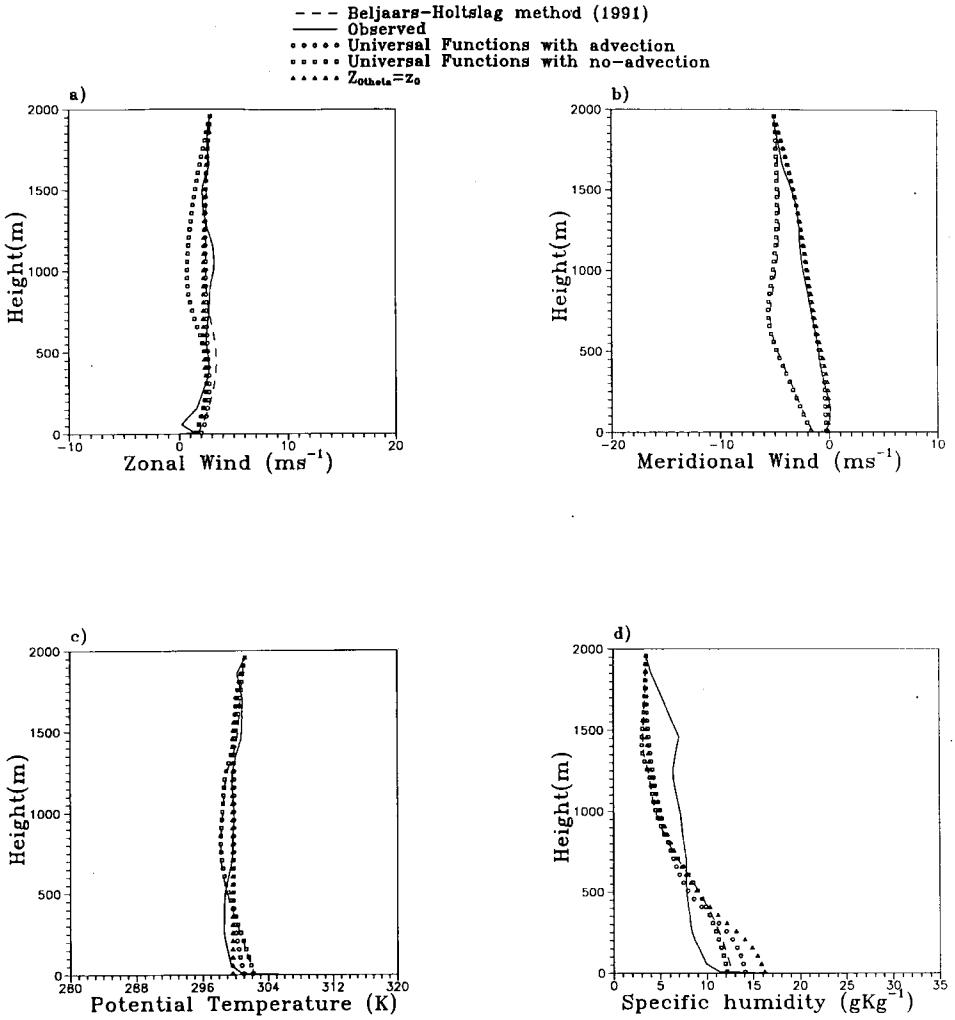

Figure 1. Vertical profiles of (a) zonal wind component (m s^{-1}), (b) meridional wind component (m s^{-1}), (c) potential temperature (K) and (d) specific humidity (g kg^{-1}) using different methods (cited in figure) at 1200 UTC on 16th February, 1997.

surface temperature gradient was noticed in Figure 4a in the order of 7 K in the first 50 m layer of the atmosphere. In Figure 4d, the temperature gradient in the first 50 m layer was 4 K. A strong inversion of 10 K is noticed in the observations at 0000 UTC of 15 February 1997 (Figure 4b), which indicated the winter characteristics. The model simulated the stable layer with less intensity. In most of the simulation hours presented above, the model predictions are in fair agreement with the observations.

The model predictions against the observations of specific humidity profiles are presented in Figures 5a–5d. One can see that overall the model predictions

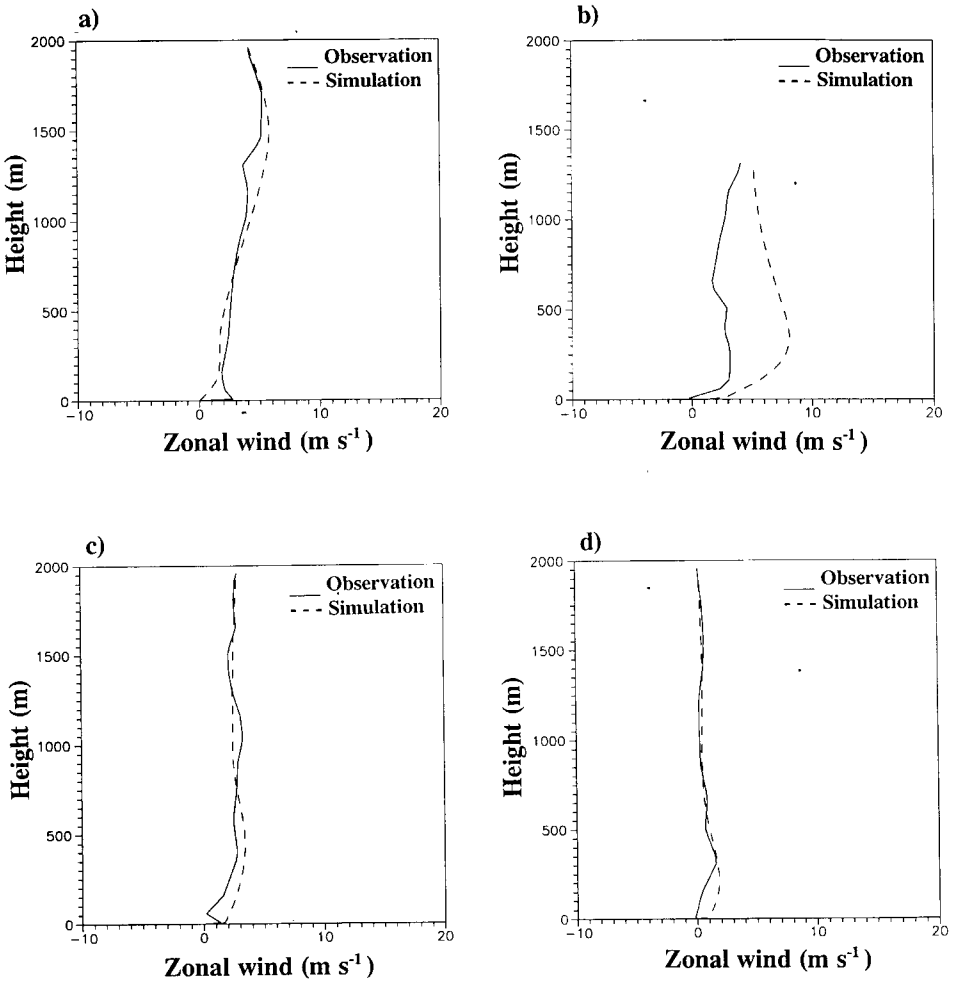

Figure 2. Vertical profiles of zonal wind component (m s^{-1}) at (a) 0900 UTC on 14th February, 1997, (b) 0000 UTC on 15th February, 1997, (c) 1200 UTC on 16th February, 1997, (d) 0300 UTC on 17th February, 1997.

TABLE II

Intervals in which the simulation results are compared with the RS/RW observations.

Date and time	Local time	Simulation hour
14th February 1997, 0900 UTC	1430 hours	9
15th February 1997, 0000 UTC	0530 hours	21
16th February 1997, 1200 UTC	1730 hours	57
17th February 1997, 0300 UTC	0830 hours	72

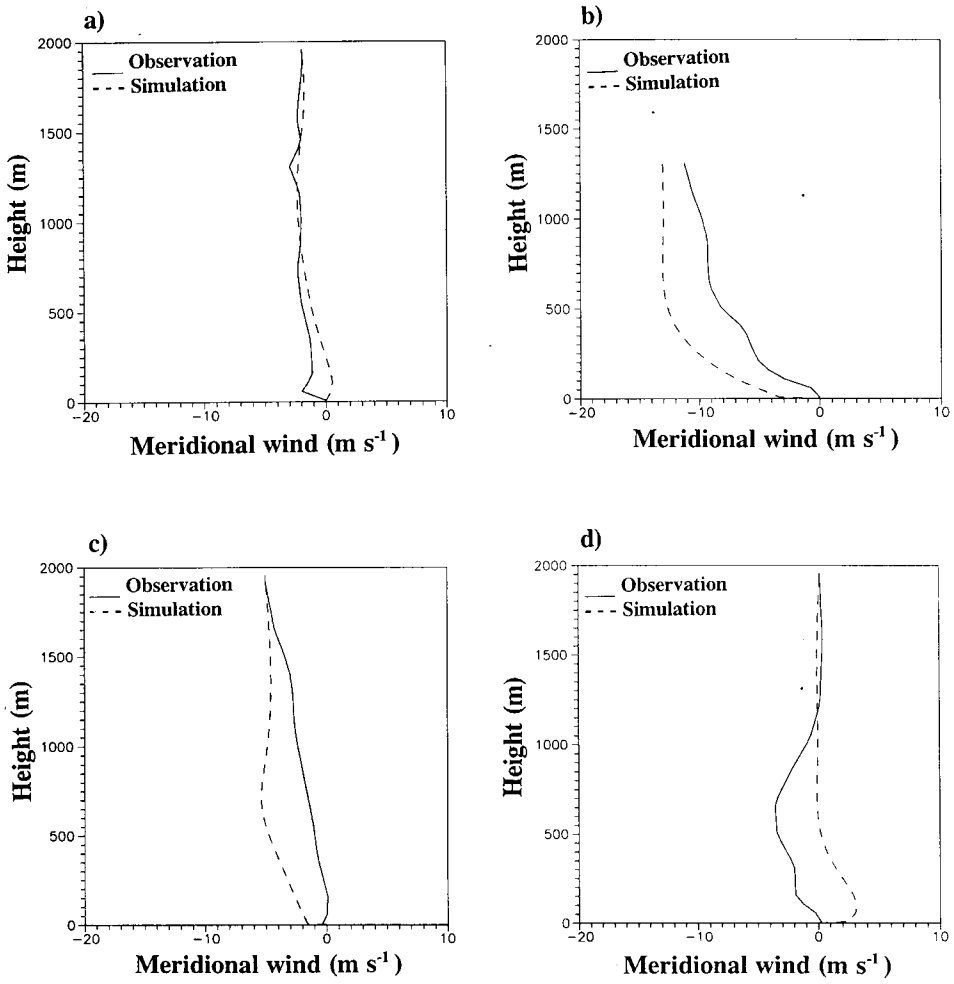

Figure 3. Vertical profiles of meridional wind component (m s^{-1}) at (a) 0900 UTC on 14th February, 1997, (b) 0000 UTC on 15th February, 1997, (c) 1200 UTC on 16th February, 1997, (d) 0300 UTC on 17th February, 1997.

are found to be in good comparison with the observations. An interesting feature is noticed in Figure 5b and Figure 5d. A sharp increase of specific humidity in the order of 3 g kg^{-1} and 5 g kg^{-1} is noticed in the first 200 m and 250 m of the atmospheric layer in Figure 5b and Figure 5d, respectively, in both the model simulations and observations. Since the period of study is during winter and the study area is a semi-arid region, one can expect strong inversions at 0000 UTC (Figure 4b) which lead to foggy conditions, which in turn result in an increase of specific humidity. But in the case of 0300 UTC (Figure 5d), even though there is a superadiabatic lapse rate at the surface (Figure 4d), a stable layer is observed from

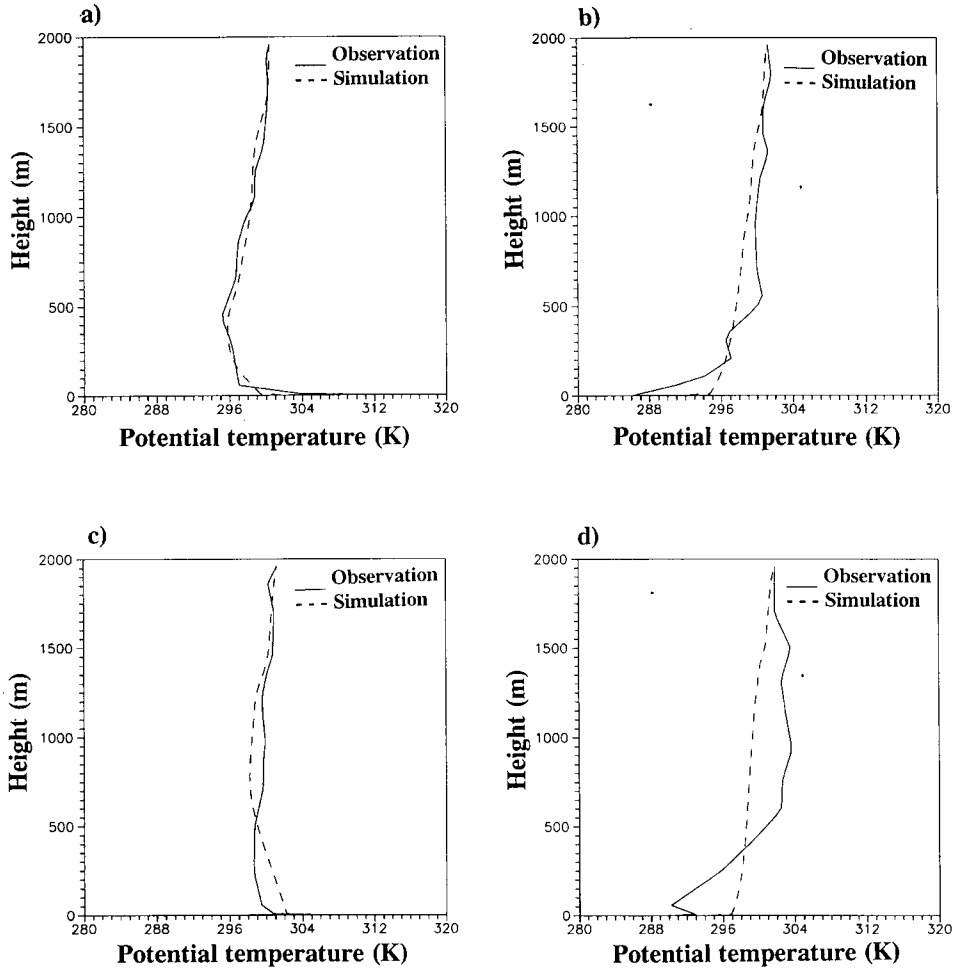

Figure 4. Vertical profiles of potential temperature (K) at (a) 0900 UTC on 14th February, 1997, (b) 0000 UTC on 15th February, 1997, (c) 1200 UTC on 16th February, 1997, (d) 0300 UTC on 17th February, 1997.

50 m onwards up to nearly 600 m and this can be attributed to the raise of specific humidity.

In Figures 6–8, the time axis is represented with 0 as 0830 hrs of 14th February, 24 as 0830 hrs of 15th February, 48 as 0830 hrs of 16th February and 72 as 0830 hrs of 17th February to show diurnal and day-to-day variations.

The diurnal and day-to-day variation of soil temperature at the surface, 5 cm, 10 cm, 20 cm, 40 cm and 100 cm depths are presented in Figures 6a– 6f. From Figure 6a, it is observed that the model slightly under-predicted the maximum and minimum temperatures. A clear cut diurnal and day-to-day variation is also observed. On 14th, 15th and 16th February, maximum surface temperature is predicted to

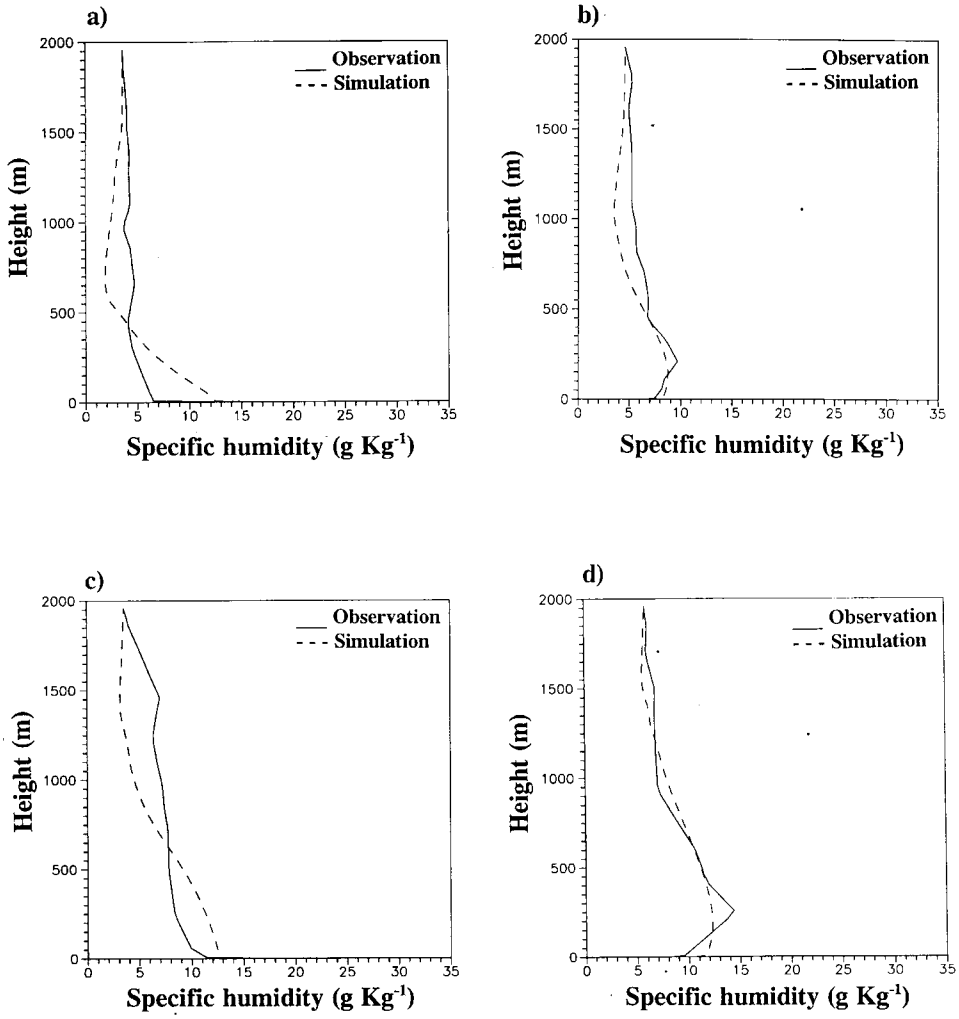

Figure 5. Vertical profile of specific humidity (g kg^{-1}) at (a) 0900 UTC on 14th February, 1997, (b) 0000 UTC on 15th February, 1997, (c) 1200 UTC on 16th February, 1997, (d) 0300 UTC on 17th February, 1997.

occur at around 1430 hrs (t = 6 hrs) and minimum temperature at around 0530 hrs (t = 21 hrs). Minimum temperatures of 12 °C on 14th, 16th and 15 °C on 15th February and a maximum temperature of 45 °C are observed. We neglected the first 12 hours of simulations in the analysis as spin up time for the model. Maximum temperatures of 39 °C on 15th and 42 °C on 16th, and minimum temperatures of 18 °C on 15th and 19 °C on 16th February, are given in model predictions.

From Figure 6b, it is found that the model prediction of peak maximum temperature is in good agreement with the observations. But the value of the minimum temperature is slightly under-predicted. In all 75 hours of model simulation, a

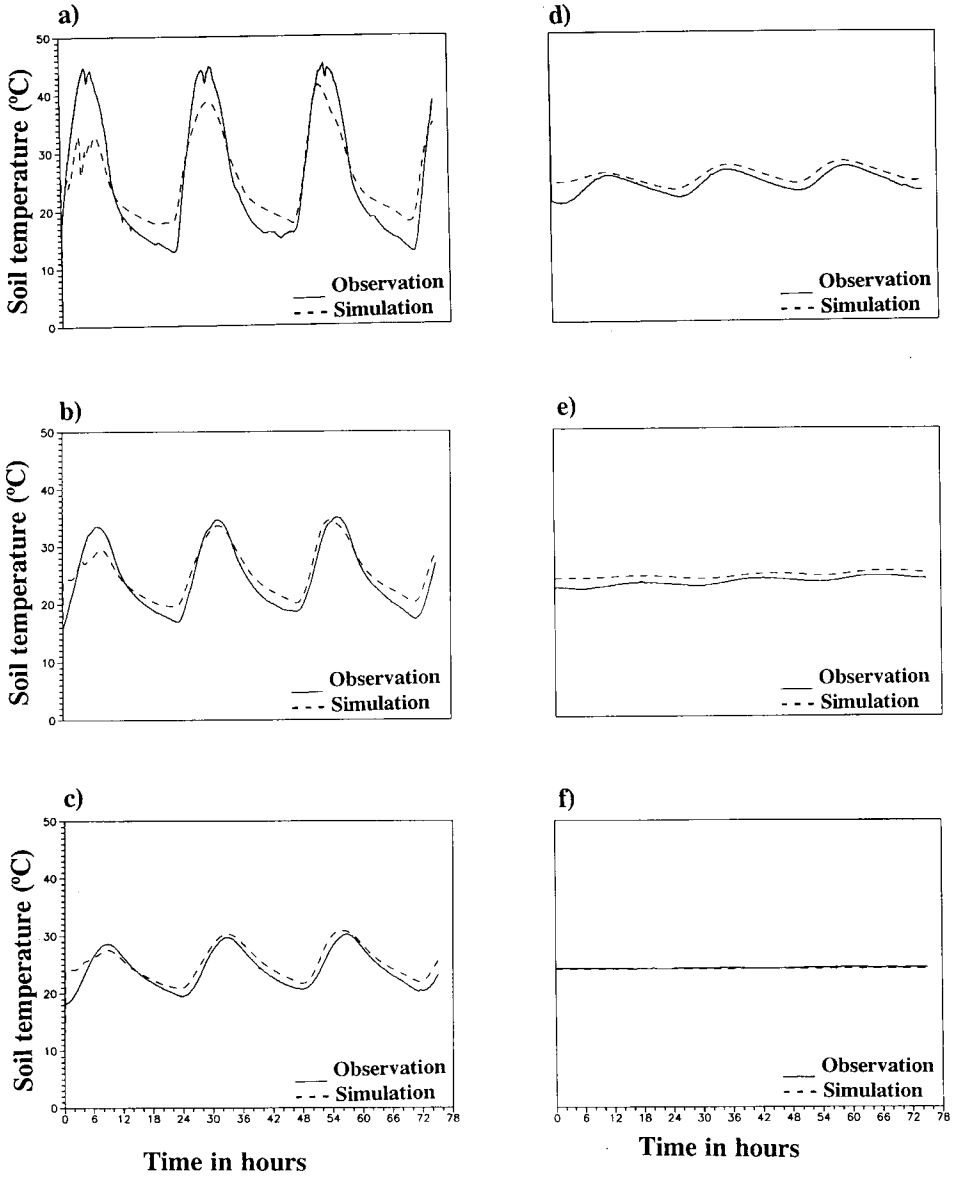

Figure 6. Diurnal and day-to-day variation of soil temperature (°C) (a) at surface, (b) 5 cm depth, (c) 10 cm depth, (d) 20 cm depth, (e) 40 cm depth, (f) 100 cm depth.

deviation of only 3 to 4 °C is noticed in minimum temperature prediction when compared with the measurements.

A slight over-prediction of maximum temperature and under-prediction of minimum temperature is noticed in Figure 6c and Figure 6d. The deviation of maximum temperature of around 1 °C is noticed between model predictions and

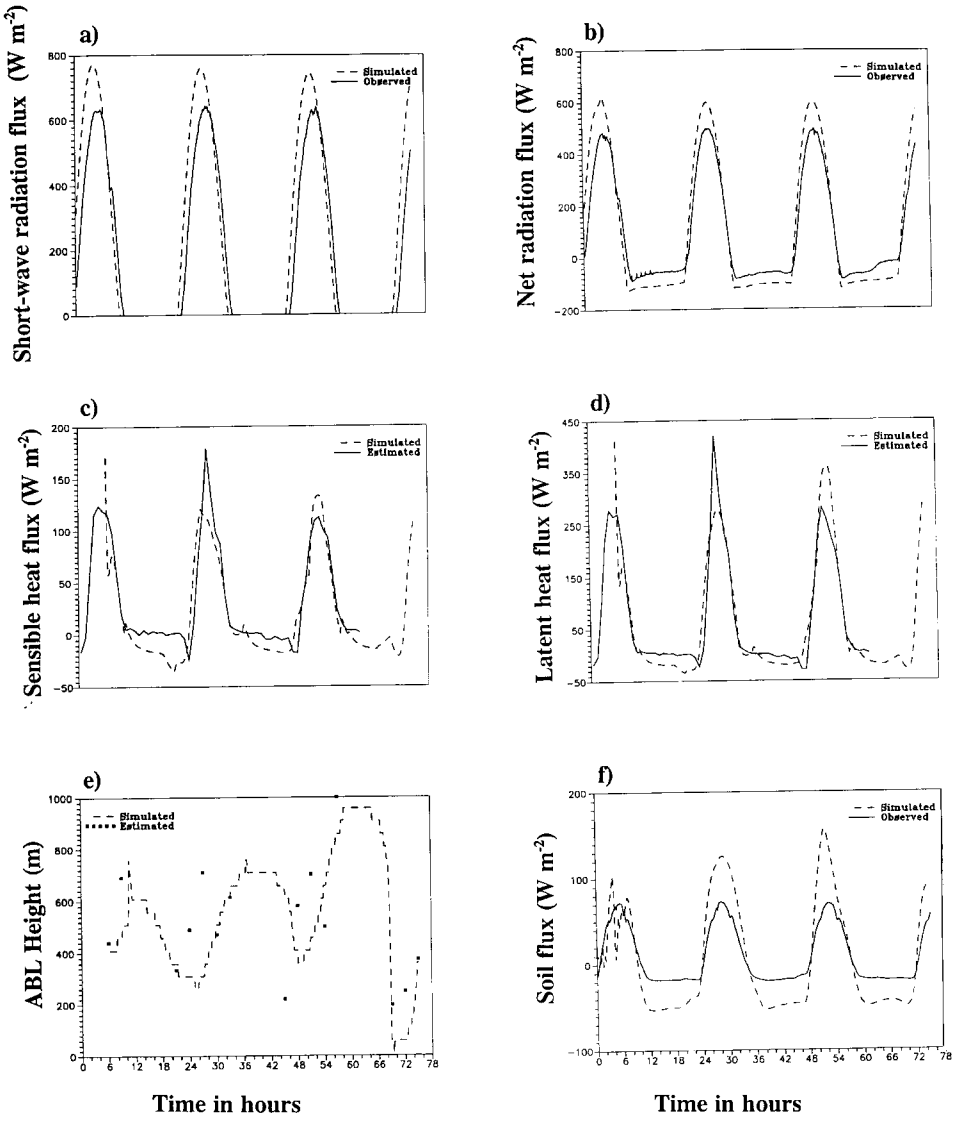

Figure 7. Diurnal and day-to-day variations of (a) shortwave radiation flux (W m^{-2}), (b) net radiation flux (W m^{-2}), (c) sensible heat flux (W m^{-2}), (d) latent heat flux (W m^{-2}), (e) PBL height (m), (f) soil heat flux (W m^{-2}).

measurements. No diurnal or day-to-day variation is seen in Figures 6e and 6f. Overall, the model predictions are in good agreement with the observations. It is noticed that the diurnal variation of surface temperature is diminishing as the depth of the soil increases.

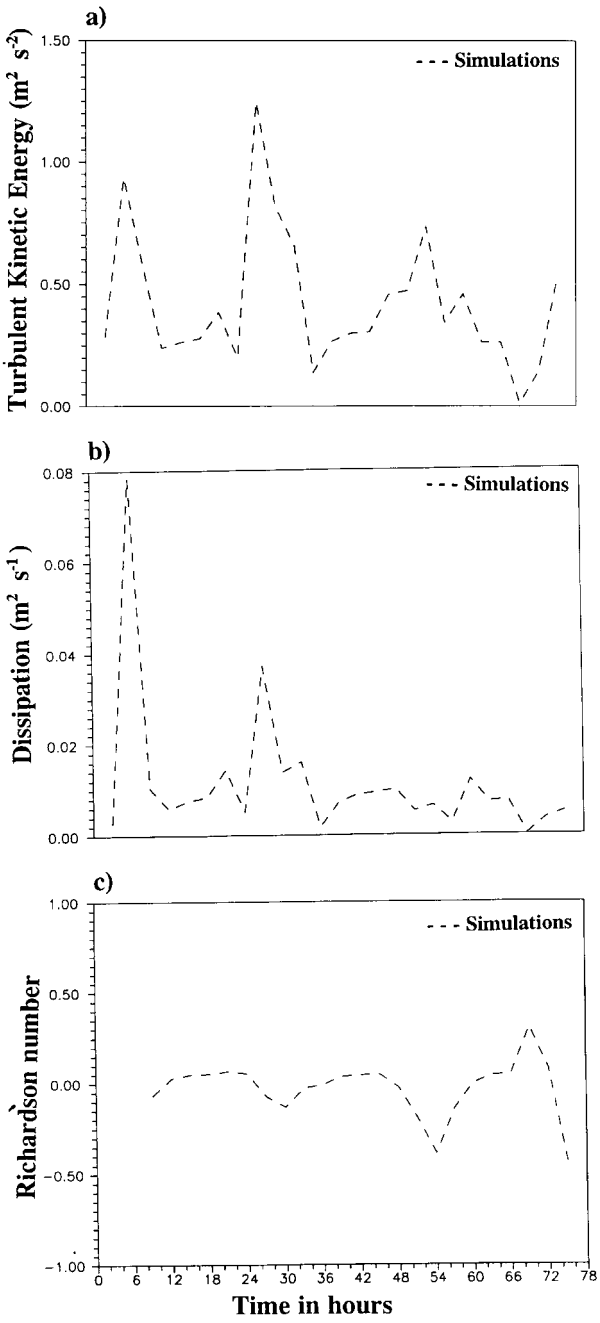

Figure 8. Diurnal and day-to-day variation of (a) turbulent kinetic enery (m^2 s^{-2}), (b) dissipation (m^2 s^{-3}), (c) Richardson number.

Figures 7a–7f represent the diurnal and day-to-day variation of fluxes of shortwave radiation, net radiation, sensible and latent heat, PBL height and soil flux at 5 cm depth respectively.

From Figure 7a, it is noticed that the maximum shortwave radiation flux is over-predicted. Maximum values of 630 W m^{-2}, 640 W m^{-2} and 650 W m^{-2} on 14th, 15th and 16th February 97, respectively, are noted. The time of occurrence of peak value matches well in the measurements and model predictions. The maximum flux is observed as well as predicted at around 1430 hrs, on both 15th and 16th February. The diurnal pattern is predicted satisfactorily.

Model predictions of diurnal and day-to-day variation of net radiation flux as seen from Figure 7b agree well with the observations. The model over-predicted the peaks of maximum and minimum net radiation flux. Deviations of 100 W m^{-2} in the maximum flux value and 30 W m^{-2} in the minimum flux between the observations and predictions are noticed. A perfect synchronization of occurrence time of maximum and minimum flux is noted among the measurements and predictions.

Model predictions of fluxes of sensible heat and latent heat at 8-m height with respect to time in LST are presented in Figures 7c and 7d. Due to the non-availability of fast response data (viz. sonic anemometer, Lyman-alpha), the fluxes of sensible heat and latent heat are estimated using tower observations by employing bulk-aerodynamic relations. These estimated fluxes are compared with the model simulations.

The diurnal and day-to-day variations of the fluxes of sensible and latent heat are predicted well. The model simulations are in good agreement with the estimated values. The maximum simulated sensible heat fluxes of 120 W m^{-2} on 15th and 135 W m^{-2} on 16th February are noted. Maximum simulated latent heat fluxes of 265 W m^{-2} and 355 W m^{-2} are noted on 15th and 16th February, respectively.

Figure 7e explains the model simulations of PBL height. Apart from the diurnal variation, a significant day-to-day variation of PBL height is noticed, with maximum PBL heights of 720 m on 15th and 960 m on 16th February. This is due to an increase in model simulations of surface soil temperature (Figure 6a), which lead to an increase in the sensible heat flux (Figure 7c) which resulted in vertical mixing and in turn enhanced the PBL height. PBL height is estimated using the observed thermodynamic profiles. The estimated PBL heights are overlaid on the simulated PBL height curve. There is a fair agreement between the estimated and the model simulated PBL heights both in terms of the actual numerical values as well as temporal variation.

Figure 7f represents the diurnal variation of soil flux at 5 cm depth. The model over-predicted the maximum and minimum peak fluxes. A maximum flux of 70–75 W m^{-2} and a minimum flux of -20 W m^{-2} are noted from the observations on 15th and 16th February, respectively while model predictions give a maximum flux of 125 W m^{-2} and 155 W m^{-2} on 16th February. A minimum flux of -55 W m^{-2} is observed on 15th and 16th February from the model simulations.

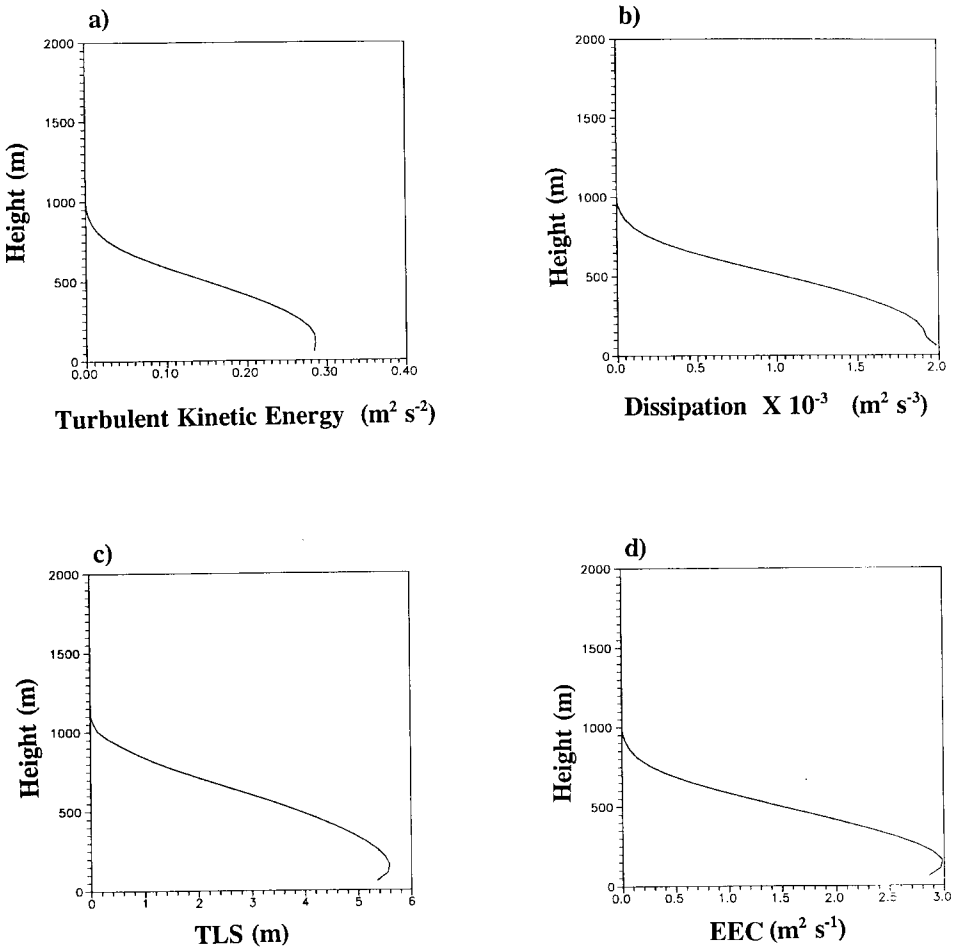

Figure 9. Simulated vertical profiles of: (a) turbulent kinetic energy ($m^2\ s^{-2}$), (b) dissipation ($m^2\ s^{-3}$), (c) turbulence length scale (m), and (d) eddy exchange coefficient for momentum ($m^2\ s^{-1}$) for 1200 UTC on 16th February, 1997.

Figures 8a–8c depict the diurnal variation of TKE, dissipation and the Richardson number (Ri) at 8-m height respectively. Model simulations at 3-hourly intervals are plotted. As explained earlier, the first 12 hours of simulations are not considered for analysis due to the spin-up process of the model.

Figure 8a explains the variation of TKE with time. The model simulation of TKE exhibits diurnal as well as day-to-day variations. Maximum values of 1.2 $m^2\ s^{-2}$ on 15th and 0.7 $m^2\ s^{-2}$ on 16th February are noted. The variation of dissipation is depicted in Figure 8b. Diurnal variation of dissipation is noticed on 15th February. No specific diurnal variation is found on 16th February.

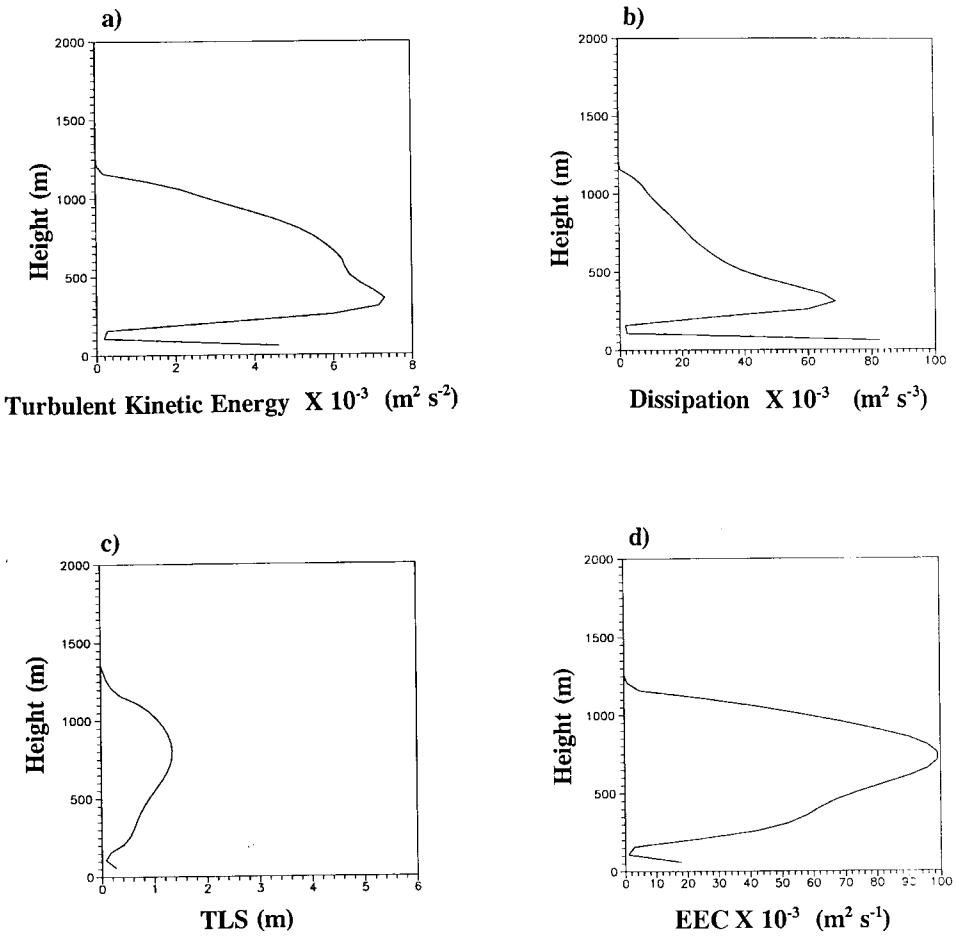

Figure 10. Simulated vertical profiles of: (a) turbulent kinetic energy ($m^2\ s^{-2}$), (b) dissipation ($m^2\ s^{-3}$), (c) turbulence length scale (m), and (d) eddy exchange coefficient for momentum ($m^2\ s^{-1}$) for 0300 UTC on 17th February, 1997.

Figure 8c depicts the model simulations of Ri. As one can expect, it shows stable conditions during the early morning and night hours and unstable conditions during daytime, in the model simulations.

The vertical profiles of model simulations of TKE, dissipation, turbulence length scale (TLS) and eddy exchange coefficient for momentum (EEC) on 16th February at 1200 UTC and 17th February at 0300 UTC are presented in Figures 9a–d and Figures 10a–d respectively. From Figures 9a–d one can see that the magnitude of TLS and EEC are well within the limits and no specific variation in the vertical is noticed. Similarly in the case of TKE and dissipation no specific change with respect to height is noticed, whereas from Figures 10a–d, a specific variation is observed. In the case of TLS and EEC, the magnitude is increasing

up to a maximum height of around 775 m and then starts decreasing. Similarly a maximum value of TKE and dissipation is noted at around 350 m height.

6. Conclusions

From the results of the numerical simulations carried out in this study the following broad conclusions may be drawn.

The model simulations of profiles of zonal and meridional wind components, potential temperature and specific humidity are in good agreement with the observations. The model well captures the daytime super-adiabatic lapse rate conditions and night time stable conditions in the first few tens of meters of the atmosphere, as revealed in the potential temperature profiles. Foggy conditions are well predicted by the model as inferred from the 0000 UTC specific humidity profiles, which is a characteristic feature of the winter period.

Soil temperature simulations at different depths are found to be in good agreement with the observations. It is observed that as depth in the soil increases, the diurnal variation diminishes, corroborating physical principles.

The diurnal and day-to-day variations of short-wave radiation and net radiation fluxes are predicted satisfactorily and found to be in good agreement with the observations. The simulations of fluxes of sensible heat and latent heat, and of PBL height are found to be consistent and explainable. The soil heat flux simulations agree well with the measurements.

The model simulations of turbulent kinetic energy exhibit diurnal variations as well as day-to-day variation whereas the model predictions of dissipation show no diurnal pattern. The stability parameter Ri is reasonably well simulated by the model. The model is able to simulate the turbulence characteristics satisfactorily.

Acknowledgements

The authors thank the Department of Science and Technology, India, and Academy of Sciences, Russia, for supporting this work under an Indo-Russia long term co-operation. V.N.L. is grateful to Prof. David Randall for the kind permission to employ his radiation code in the PBL model. The authors also thank the Indian Institute of Tropical Meteorology, Pune for providing the data. Finally, the authors are indebted to the anonymous referees and the editor for their helpful comments. This work has been partially supported by the Council for Scientific and Industrial Research, India and from the Project INTAS 961-1935 and by the Russian Fund for Basic Research (Grant # 98-05-64210).

References

Aupoix, B., Cousteau, J., and Liandrat, J.: 1989, 'MIS: A Way to Derive the Dissipation Equation', *Turbulent Shear Flows* **6**, 6–17.

Beljaars, A. C. M. and Holtslag, A. A. M.: 1991, 'Flux Parameterization over Land Surfaces for Atmospheric Models', *J. Appl. Meteorol.* **30**, 327–341.

Businger, J. A., Wyngaard, J. C., Izumi, I., and Bradley, E. F.: 1971, 'Flux Profile Relationships in the Atmospheric Surface Layer', *J. Atmos. Sci.* **28**, 181–189.

Carl, M. D., Tarbell, T. C., and Panofsky, H. A.: 1973, 'Profiles of Wind and Temperature from Towers over Homogeneous Terrain', *J. Atmos. Sci.* **30**, 788–794.

Deutsches Klimazentrum (DKRZ): 1992, 'The ECHAM3 Atmospheric General Circulation Model', Tech. Rep., No. 6, Hamburg, 188 pp.

Fairall, C. W., Bradley, E. F., Rogers, D. P., Edson, J. B., and Young, G. S.: 1996, 'Bulk Parameterization of Air-Sea Fluxes for Tropical Ocean Global Atmosphere Coupled Ocean Atmosphere Response Experiment', *J. Geophys. Res.* **101**(C2), 3747–3764.

Garratt, J. R. and Hicks, B. B.: 1973, 'Momentum, Heat and Water Vapor Transfer to and from Natural and Artificial Surfaces', *Quart. J. Roy. Meteorol. Soc.* **99**, 680–689.

Harshavardhan, Roger, D., Randall, D. A., and Corsetti, T. G.: 1987, 'A Fast Radiation Parameterization for Atmospheric Circulation Models', *J. Geophys. Res.* **92**, 1009–1016.

Kazakov, A. L. and Lykossov, V. N.: 1982, 'On Parameterization of Interaction between the Atmosphere and Underlying Surface in Numerical Modeling of Atmospheric Processes', *Proc. West-Siberian Inst., Gidrometeoizdat, Moscow* **55**, 3–20 (in Russian).

Kolmogorov, A. N.: 1942, 'Incompressible Fluid Turbulent Motion Equations', *Izv. Akad. Nauk SSSR, Ser. Fiz.* **6**, 56–58.

Kusuma, G. Rao, Lykossov, V. N., Prabhu, A., Sridhar, S., and Tonkacheyev, E.: 1996, 'The Mean and Turbulence Structure Simulation of the Monsoon Trough Boundary Layer Using a One-Dimensional Model with $e - l$ and $e - \epsilon$ Closures', *Proc. Indian Acad. Sci. (Earth Planet. Sci.)* **105**, 227–260.

Kusuma, G. Rao, Sethu Raman, Prabhu, A., and Narasimha, R.: 1995, 'Turbulent Heat Flux Variation over the Monsoon Trough Region during MONTBLEX-90', *Atmos. Environ.* **29**, 2113–2129.

Lykossov, V. N. and Platov, G. A.: 1992, 'A Numerical Model of Interaction between Atmospheric and Oceanic Boundary Layers', *Russ. J. Numer. Anal. Math. Modelling* **7**, 419–440.

Mihailovic, D. T., Pielke, R. A., Rajkovic, B., Lee, T. J., and Jeftic, M.: 1993, 'A Resistance Representation of Schemes for Evaporation from Bare and Partly Plant Covered Surfaces for Use in Atmospheric Models', *J. Appl. Meteorol.* **32**, 1038–1054.

Noilhan, J. and Planton, S.: 1989, 'A Simple Parameterization of Land Surface Processes for Meteorological Models', *Mon. Wea. Rev.* **117**, 536–549.

Panofsky, H. A. and Dutton, J. A.: 1984, 'Atmospheric Turbulence. Models and Methods for Engineering Applications', Wiley-Interscience Publ., New York, 397 pp.

Parashuram, Venugopal, T. and Mohanty, U. C.: 1994, 'Simulation of the Thermodynamic Structure of Atmospheric Boundary Layer over Calcutta with a 1-D TKE Closure PBL Model', *Mausam* **45**, 107–114.

Paulson, C. A.: 1970, 'The Mathematical Representation of Wind Speed and Temperature Profiles in the Unstable Atmospheric Surface Layer', *J. Appl. Meteorol.* **9**, 857–861.

Pielke, R. A.: 1984, 'Mesoscale Meteorological Modeling', Academic Press, New York, 612 pp.

Potty, K. V. J., Mohanty, U. C., Nandi, B., and Ramesh, K. J.: 1996, 'Planetary Boundary Layer over Monsoon Trough Region in a High Resolution Primitive Equation Model', *Proc. Indian Acad. Sci. (Earth Planet. Sci.)* **105**, 81–100.

Raman, S., Mohanty, U. C., Reddy, N. C., Alapaty, K., and Madala, R. V.: 1998, 'Numerical Simulation of the Sensitivity of Summer Monsoon Circulation and Rainfall over India to Land Surface Processes', *Pure Appl. Geophys.* **152**, 781–809.

Sellers, P. J., Randall, D. A., Collatz, G. J., Berry, J. A., Field, C. B., Dazlich, D. A., Zhang, C., Collelo, G. D., and Bounoua, L.: 1996, 'A Revised Land Surface Parameterization (SiB2) for Atmospheric GCMs. Part 1. Model Formulation', *J. Climate* **9**, 676–705.

Stull, R. B.: 1988, 'An Introduction to Boundary Layer Meteorology', Kluwer Academic Publishers, Dordrecht, 666 pp.

Tyagi, A., Mohanty, U. C., and Ramesh, K. J.: 1994, 'Planetary Boundary Layer Structure in the Monsoon Trough Region', *Mausam* **45**, 213–222.

Vernekar, K. G., Mohan Brij, Saxena, S., and Patil, M. N.: 1993, 'Characteristics of the Atmospheric Boundary Layer over a Tropical Stations as Evidenced by Tethered Balloon Observations', *J. Appl. Meteorol.* **32**, 1426–1432.

Vernekar, K. G., Sadani, L. K., Mohan Brij, Saxena, S., Debaje, S. B., Pillai, J. S., Murthy, B. S., and Patil, M. N.: 1991, 'Structure and Growth of Atmospheric Boundary Layer as Observed by Tethered Balloon Payload', *Indian J. Radio Space Phys.* **20**, 312–315.

Volodin, E. M. and Lykossov, V. N.: 1998, 'Parameterization of Heat and Moisture Transfer in the Soil-Vegetation System for Use in Atmospheric General Circulation Models: 1. Formulation and Simulations Based on Local Observational Data', *Izvestiya, Atmos. Ocean Phys.* **34**, 453–465.

Xu, D. and Taylor, P. A.: 1997, 'An $E-\epsilon-l$ Closure Scheme for Planetary Boundary-Layer Models: the Neutrally Stratified Case', *Boundary-Layer Meteorol.* **84**, 247–266.